

RESEARCH

Open Access



Targeting BMI-1 with PLGA–PEG nanoparticle-containing PTC209 modulates the behavior of human glioblastoma stem cells and cancer cells

Elham Poonaki^{1,2}, Fatemeh Ariakia^{2,3}, Mohammad Jalili-Nik^{4,5†}, Mehdi Shafiee Ardestani¹, Gholamhossein Tondro⁶, Fariborz Samini⁷, Sepideh Ghasemi⁸, Sajad Sahab-Negah^{2,3,8*} and Ali Gorji^{2,3,8,9,10*}

*Correspondence:

sahabnegahs@mums.ac.ir;
gorjia@uni-muenster.de
†Elham Poonaki, Fatemeh Ariakia and Mohammad Jalili-Nik contributed equally to this work

² Neuroscience Research Center, Mashhad University of Medical Sciences, Mashhad, Iran
Full list of author information is available at the end of the article

Abstract

Despite advances in glioblastoma (GBM) treatments, current approaches have failed to improve the overall survival of patients. The oncogene BMI-1, a core member of the polycomb group proteins, is a potential novel therapeutic target for GBM. To enhance the efficacy and reduce the toxicity, PTC209, a BMI-1 inhibitor, was loaded into a PLGA–PEG nanoparticle conjugated with CD133 antibody (Nano-PTC209) and its effect on the behavior of human GBM stem-like cells (GSCs) and the human glioblastoma cell line (U87MG) was assessed. Nano-PTC209 has a diameter of ~75 nm with efficient drug loading and controlled release. The IC₅₀ values of Nano-PTC209 for GSCs and U87MG cells were considerably lower than PTC209. Nano-PTC209 significantly decreased the viability of both GSCs and U87MG cells in a dose-dependent manner and caused a significant enhancement of apoptosis and p53 levels as well as inhibition of AKT and JNK signaling pathways. Furthermore, Nano-PTC209 significantly inhibited the migration ability, decreased the activity of metalloproteinase-2 and -9, and increased the generation of reactive oxygen species in both GSCs and U87MG cells. Our data indicate that PLGA–PEG nanoparticle conjugated with CD133 antibody could be an ideal nano-carrier to deliver PTC209 and effectively target BMI-1 for potential approaches in the treatment of GBM.

Keywords: Brain tumor, Metastasis, Nanoparticles, Scaffold, Cancer

Background

Glioblastoma multiforme (GBM), the most common malignant brain tumor, is a highly aggressive cancer with extremely poor clinical outcomes (Hanif et al. 2017). Despite advances in therapeutic strategies, current treatments have failed to improve the overall survival of patients with GBM (Qazi et al. 2017). Human B cell-specific Moloney murine leukemia virus integration site 1 (BMI-1), a key member of the polycomb repressive complex 1 and a transcription regulator, maintains stem cell self-renewal and implicates in a variety of human cancer types, including GBM (Wang et al. 2015; Di Croce 2013;



© The Author(s) 2021, corrected publication February 2021. This article is licensed under a Creative Commons Attribution 4.0 International License, which permits use, sharing, adaptation, distribution and reproduction in any medium or format, as long as you give appropriate credit to the original author(s) and the source, provide a link to the Creative Commons licence, and indicate if changes were made. The images or other third party material in this article are included in the article's Creative Commons licence, unless indicated otherwise in a credit line to the material. If material is not included in the article's Creative Commons licence and your intended use is not permitted by statutory regulation or exceeds the permitted use, you will need to obtain permission directly from the copyright holder. To view a copy of this licence, visit <http://creativecommons.org/licenses/by/4.0/>. The Creative Commons Public Domain Dedication waiver (<http://creativecommons.org/publicdomain/zero/1.0/>) applies to the data made available in this article, unless otherwise stated in a credit line to the data.

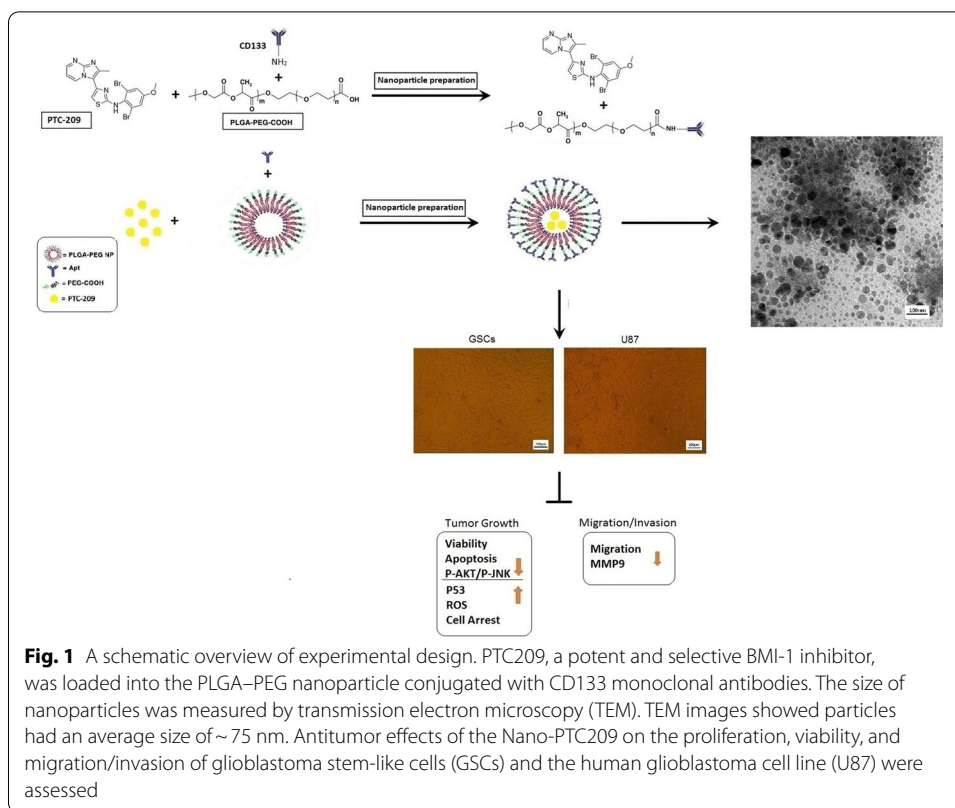
Hong et al. 2015). The mean value of BMI-1 expression is markedly upregulated in GBM and inhibits the activation of the tumor-suppressor signaling pathway (Yoshimoto et al. 2011). Furthermore, the expression of BMI-1 has considerably upregulated in glioblastoma stem-like cells (GSCs) and acts as a key regulator of their self-renewal and differentiation (Hong et al. 2015). The selective inhibition of post-transcriptional regulation of BMI-1 significantly impairs GSCs proliferation and differentiation *in vitro* and reduces GBM growth *in vivo* (Kong et al. 2018). Furthermore, the expression of the CD133, a glycoprotein antigen, in GBM correlates with tumor progression and patient survival (Lim et al. 2014). CD133 antigen is crucial for the oncogenic potential of GSCs as its silencing inhibits GSC self-renewal and tumorigenic capacities (Shevchenko et al. 2020). BMI-1 is expressed in human GBM tumors and highly enriched in CD133-positive cells (Abdoun et al. 2009; Venugopal et al. 2012). The association of CD133 and BMI-1 functions and their potential as targets for tackling GBM treatment-resistant cells have been reported (Vora et al. 2019). Silencing BMI-1 led to the elimination of the tumor-forming capacity of CD133⁺ GBM cells (Baxter et al. 2014).

PTC209, a potent and selective inhibitor of BMI-1, inhibits post-transcriptional regulation of BMI-1, down-regulates BMI-1 production (Kreso et al. 2014), and exerts strong antitumor effects on various cancer cells, including acute myeloid leukemia, biliary tract, myeloma, squamous cell carcinoma, glioblastoma, lung, breast, colon, and GBM (Wang et al. 2017; Kong et al. 2018). PTC209 inhibits tumor growth mainly through the induction of apoptosis and cell cycle arrest, particularly by action on CD133⁺ tumor cells (Wang et al. 2017; Kong et al. 2018; Sulaiman et al. 2019). However, high toxicity and restricted transport across the blood–brain barrier could limit the potential therapeutic utility of PTC209 (Pardridge et al. 2015; Srinivasan et al. 2017; Kong et al. 2018). Nano-carrier-based drug delivery is a potential novel therapeutic strategy for GBM (Agarwal et al. 2019; Liao et al. 2019; Sahab-Negah et al. 2020). Polymeric drug delivery systems have been developed to enhance drug stability, decrease toxic side effects, promote targeting ability, and improve the therapeutic efficacy in cancer therapy (Wait et al. 2015; Senapati et al. 2018; Granz and Gorji 2020; Sahab-Negah et al. 2020). Polyethylene glycol–polylactic acid-co-glycolic acid (PEG–PLGA) copolymers exhibit promising potential in targeted drug delivery systems as tumor-targeting nanocarriers (Zhang et al. 2014; Agarwal et al. 2019). The present study aimed to investigate the effect of PTC209 loaded into a PLGA–PEG nanoparticle conjugated with CD133 antibody (Nano-PTC209) on the survival, proliferation, migration, and invasive properties of human GSCs and the human glioblastoma cell line (U87MG). Furthermore, the signal transduction pathways mediating Nano-PTC209 effects on GSCs and U87MG cells were investigated.

Materials and methods

Study design and ethical statement

To improve the efficacy of PTC209, PLGA–PEG nanoparticles conjugated with anti-CD133 monoclonal antibody was designed. As shown in Fig. 1, PTC209 was loaded into the nanoparticles and the size of particles was measured by transmission electron microscopy (TEM). In the next step, GSCs derived from GBM tissues of two patients as well as U87MG cells were cultured and treated with Nano-PTC209. To determine the anti-tumor effects of Nano-PTC209, tumor growth and migration/invasion ability



of GSCs and U87MG cells were assessed in vitro. Ethical approval was obtained from the Ethics Committee of Shefa Neuroscience Research Center, Tehran, Iran. All samples were collected after informed written consent from patients.

Preparation of PTC209-loaded PLGA–PEG nanoparticle conjugated with anti-CD133 monoclonal antibody

The PLGA microsphere (50:50, 50.000–75.000, 430471—Sigma-Aldrich, Germany) was prepared based on a double emulsion solvent evaporation approach using water-in-oil-in-water at room temperature. Next, the PLGA (25 mg) was suspended in ethyl acetate (5 ml) by 1 ml of phosphate buffer saline (PBS; pH = 7.4) including N-cetyl-N,N,N-trimethyl ammonium bromide (Merck, USA) (0.2%, w/v) and then sonicated in 50 watts and remained on Stirrer for 7 days to be solved appropriately. Thereafter, an appropriate dose of PEG (3 k) based on a mixture of COOH–PEG–NH₂ to PLGA–COOH was added to the solvent in the presence of 2-ml methylene chloride to remove water from the reaction. PLGA was dissolved by 1-ethyl-3-(3-dimethyl aminopropyl)-carbodiimide (EDC) and dichloromethane. A combination of methanol-ethyl was added to the emulsion to remove excess EDC. The nanoparticle was stirred with CD133 monoclonal antibody for 1 week on a magnetic stirrer and cool condition. Then, PTC209 (Sigma-Aldrich, Germany) was dissolved in dimethyl sulfoxide (DMSO; Sigma-Aldrich, Germany) and loaded into nanoparticles for 6 h. Finally, the prepared sample was filtered by a 0.22-μm filter to remove probable contaminations and stored at 4 °C until use.

Characterization of Nano-PTC209

TEM and dynamic light-scattering (DLS) studies

Physicochemical features of Nano-PTC209, including the size and distribution of particles, were analyzed by TEM and DLS methods. Analysis of nanoparticle morphology was performed by TEM. Briefly, after diluting of nanoparticles suspension with deionized water, 2% uranyl acetate was added to the suspension for 2 min. Then, the suspension was sonicated in an ultrasound bath at room temperature for 1 min. Next, the sample was placed on a copper mesh and dried at room temperature. Ultimately, images were taken using a Philips CM10 TEM. We also measured the size distribution of Nano-PTC209 using Zeta-sizer Nano ZS (Malvern Instruments Ltd., UK). Nano-PTC209 was diluted with deionized water (1:10) and the sample size was assessed with the DLS method. The distribution of size was estimated by the polydispersity index.

Fourier Transform Infrared Spectroscopy (FTIR)

FTIR was performed to evaluate the chemical interactions and the compatibility of Nano-PTC209. Nano-PTC209 (2 mg) was poured on the KBr disc container. KBr did not induce any peaks at the wave of 650–4000 cm^{-1} and is appropriate for the spectroscopy of organic substances, including FTIR. The analysis was carried out by recording the absorbance, which could lead to the appearance of different peaks. The vibrational frequency of atoms in the functional groups of the compound was represented in the specific wavelength. FTIR assessment was performed using Nicolet OMNIC Software (Thermo Fisher Scientific, Inc., Germany).

In vitro drug release

Drug release evaluation was performed with 100 mg of nanoparticles suspended in 1 ml PBS (pH 7.4, 0.1 M) containing 10% fetal bovine serum (FBS). PBS is one of the most simple and common media for release kinetics studies (Abouelmagd et al. 2015). Nanoparticles (10 ml) were placed in a dialysis bag and the tubes were transferred into vials containing PBS with or without 10% FBS (Guo et al. 2017). Then the microtubules were placed in a shaker incubator at 37 °C (100 rpm) and the amount of released PTC209 in the dialysate was assessed at various intervals (1, 2, 4, 8, 12, 24, 48, 72, 96, and 120 h) by high-performance liquid chromatography. After centrifuging the suspensions (12,000 $g \times 40$ min) at 25 °C, the supernatant was subjected to be assessed with an ultraviolet spectrophotometer at 562 nm. After each sampling, an equal new buffer (PBS or PBS + 10% FBS) was added to the tubes.

GSCs and U87MG cell culture

Primary glioblastoma tissues were collected during tumor resection from two patients who suffered from GBM. After mechanically and enzymatically digesting of tissues, single cells were cultured in Dulbecco's modified Eagle's medium/F12 (Gibco, Germany) composed of 0.5% N2 supplement (Gibco, Germany), 2 $\mu\text{g}/\text{ml}$ heparin (Sigma-Aldrich, Germany), 1% glutamine (Invitrogen, USA), 3% B27 supplement (Invitrogen, USA), 20 ng/ml epidermal growth factor (Miltenyi Biotec, Germany), 10 ng/ml basic

fibroblast growth factor (Millipore, Germany), and 1% penicillin/streptomycin (Gibco, Germany). The U87MG cells were expanded in Eagle's Minimum essential medium with fetal bovine serum (10%). Cells used in all experiments were between passage 5 and 8. Cells were incubated in a 37 °C humidified incubator of 5% CO₂.

Self-renewal capacity of GSCs

To detect self-renewal capacity, neurosphere assay and immunocytochemistry were performed. The number of neurospheres was assessed for 3–5 culture passages. The proliferation capacity was also evaluated by the expression of Ki67, nestin, and glial fibrillary acidic protein (GFAP) (Santa Cruz, Germany). For this purpose, GSCs were fixed by 4% formaldehyde for 30 min. After rinsing with PBS, permeabilization and blocking were performed using Triton X-100 solution (0.1%) and incubated with 5% bovine serum albumin at room temperature. Then, the primary antibodies (mouse anti-nestin, mouse anti-GFAP, rabbit anti-Ki67) were incubated overnight at 4 degrees (Table 1). Subsequently, the cells were washed with PBS and then incubated with goat anti-mouse IgG (FITC) or goat anti-rabbit IgG (FITC) for 1 h at 4 °C. Nuclei were stained using 4',6-diamidino-2-phenylidole dihydrochloride (DAPI). In control studies, the primary antibody was replaced with mouse or rabbit control IgG. There was no immunoreactivity in these controls.

GSC characterization

The expressions of nestin (Santa Cruz, Germany), as a neural progenitor marker, and GFAP (Santa Cruz, Germany), as a proliferative/developing astrocyte marker, were assessed using flow cytometry. After passage 3, GSCs were collected using centrifugation, the cell pellet was washed with PBS and 1% bovine serum albumin and incubated with the specific antibody at concentrations recommended by the manufacturers. The antibodies were including FITC-conjugated anti-CD44, phycoerythrin (PE)-conjugated anti-CD34, and FITC-conjugated anti-CD45. Finally, the cells were analyzed using Cell Quest Software on FACS flow cytometry (Becton Dickinson, UK) (23). Relevant isotype controls and unstained samples were used for each antibody. FITC-conjugated

Table 1 Summary of antibodies used in immunocytochemistry and western blotting

Primary antibody	Cell target	Dilution	Clonality	Host species	Company	Secondary antibody
Ki67	Proliferation marker	1:100	Polyclonal	Rabbit	Abcam	Goat
Nestin	Neural stem cells	1:50	Monoclonal	Mouse	Santa Cruz	Goat
GFAP	Glial Tumor cells	1:300	Monoclonal	Mouse	Sigma	Goat
CD34	Endothelial cells	1:20	Monoclonal	Human	eBioscience	Mouse
CD44	Cancer progenitor cells	1:50	Monoclonal	Human	eBioscience	Rat
CD45	Hematopoietic stem cells	1:20	Monoclonal	Mouse	eBioscience	Goat
<i>NF-kB-p65</i>	Mammalian cells	1:1000	Polyclonal	Rabbit	Abcam	Goat
<i>p-Akt</i>	Mammalian cells	1:1000	Polyclonal	Rabbit	Cell signaling	Goat
<i>p-SAPK/JNK</i>	Mammalian cells	1:1000	Polyclonal	Rabbit	Cell signaling	Goat
β -Actin	Mammalian cells	1:1000	Monoclonal	Rabbit	Cell signaling	Goat

anti-CD44 and FITC-conjugated anti-CD45 were read separately for avoiding interference between the two channels (Table 1).

Determination of the half-maximal inhibitory concentration (IC50)

To determine the IC₅₀ of Nano-PTC209 on GSCs and U87MG cells, the MTT assay was performed. The cells were seeded in a 96-well culture plate overnight at 37 °C. These cells were exposed to Nano-PTC209 or PTC209 for 24 and 48 h. After adding the MTT solution (10 µl) in PBS (5 mg/ml) for 4 h to each well, the supernatants were discarded, and DMSO (100 µl) was used to dissolve the formazan crystals. Finally, the plates were gently shaken for 60 min in a dark condition, and absorbance was measured at 545 and 630 nm using a plate reader (Stat FAX303). IC₅₀ was calculated by linear regression analysis (Sebaugh 2011).

Cell viability method

Evaluation of cell viability was performed by LIVE/DEAD Viability/Cytotoxicity Kit (Invitrogen, USA) (Sahab Negah et al. 2020). Cells were cultured in 96 adherent's well plates and incubated at 37 °C with 5% CO₂. Then, the cells were treated with Nano-PTC209 (130 and 260 nM for GSCs; 68.5 and 137 nM for U87MG) for 24 h. After treatment, 100 µl LIVE and DEAD reagent (containing 2 µM Calcein-AM and 4 µM of EthD-1 in PBS) was added to cells in a dark condition for 30 min at 37 °C. To detect live/dead cells, images were obtained by the ZEISS Axiovert fluorescent microscope (Zeiss, Germany). The percentage of live cells was detected by ImageJ software.

Assessment of reactive oxygen species (ROS)

The production of ROS was visualized by the H2DCFDA cellular ROS detection assay kit (Abcam, UK). The GSCs and U87MG cells were cultured on a poly-L-lysine coated 96-well plate. Then, the wells were treated with Nano-PTC209 (130 and 260 nM for GSCs; 68.5 and 137 nM for U87MG) at the predetermined time points (4, 8, and 24 h). Next, cells were washed with PBS and were kept in a dark condition with 100 µl of H2DCFDA (25 µM) solution at 37 °C for 30 min. Images were visualized and analyzed using the ZEISS Axiovert fluorescent microscope (Zeiss, Germany).

Apoptosis assay

To detect whether Nano-PTC209 can induce apoptosis and necrosis in GSCs and U87MG, Annexin V/PI double-staining reagent (Cayman, USA) was applied in flow cytometric analyses. The cells were cultured onto a 6-well plate at the density of 1×10^6 and treated with IC₅₀ concentration of Nano-PTC209 for 24 h. Then, cells after washing with $1 \times$ binding buffer and centrifuging at 400 g for 5 min were treated with 50 µl of annexin-V and propidium iodide (PI) in a dark condition at room temperature for 15 min in the falcon tubes (12 × 75 mm, polystyrene round-bottom) in 100 µl of suspension. Finally, the volume of cells was set at 250 µl with a 1X binding buffer. A FACSCAL-IBUR™ FLOW CYTOMETER (Becton Dickinson, USA) was used to evaluate the cells. The data were evaluated by the software FlowJo version 10 (Flowjo, USA).

Cell cycle arrest

GSCs and U87MG cells were seeded and treated with different concentrations of Nano-PTC209 in 6-well plates for 24 h and fixed in ethanol (70%) at -20°C overnight. Then, the cells were treated with RNase A (100 μl) for 30 min and incubated in PI/Triton X-100 solution composed of 50 $\mu\text{g/ml}$ PI, 1 mg/ml sodium citrate, and 0.1% Triton X-100 for 30 min. Then, the cell cycle was evaluated for 1×10^4 cells by a FACSCALIBUR™ FLOW CYTOMETER (Becton Dickinson, USA). The data were assessed by the software FlowJo version 10 (Flowjo, USA).

Quantitative real-time polymerase chain reaction (RT-PCR) assay

To assess the effect of Nano-PCT209 on the expression of p53, GSCs and U87MG cells were cultured in 6-well plates (1×10^6 /well) and treated with the IC50 concentration of Nano-PCT209 for 24 h. Using the RNeasy® mini kit (Qiagen, Germany), total RNA extraction was carried out. Next, the Revert-Aid First Strand cDNA Synthesis (Thermo Fisher Scientific, Germany) was used for reverse transcription of RNA. The quantitative RT-PCR (qRT-PCR) assessment was carried out using RealQ Plus 2X-MasterMix Green without Rox™ (Amplicon, Denmark). qRT-PCR was performed with selected primer for p53. The cDNA amplification was performed using the Light-Cycler 96 real-time PCR system (Roche, USA). GAPDH was used for a housekeeping gene. Using the Livak method, the relative expression of genes was assessed.

Western blotting analysis

The GSCs and U87MG cells (1×10^6 cells/well) were cultivated in a 6-well plate and treated with the IC50 concentration of Nano-PTC209 for 24 h. Then, cells were exposed to cell lysis buffer (0.1 M NaCl, 0.01 M Tris, and 0.1 mM EDTA) as well as a protease inhibitor and centrifuged at 13×10^3 rpm for 15 min. Based on the standard Bradford method, the supernatant was utilized for the detection of total protein concentration. To transfer protein into polyvinylidene fluoride (PVDF) membrane, the gel containing the sample was located in a semi-dry Western blotting apparatus. Then, the PVDF membrane was incubated in a shaker incubator with primary antibodies (NF- κB p65, phospho-SAPK/c-Jun N-terminal kinases (JNK), phospho-Akt, and β -actin; Table 1). Then, secondary antibody horseradish peroxidase conjugated (1:1000; Santa Cruz, Germany) was used. Using the chemiluminescence kit (Fermentase, Germany), western blot analyses were conducted. The intensity of each band was evaluated by Image J software and based on the percentage of existent bands compared with the control bands.

Wound-healing assay

The migration assay was evaluated by a wound-healing approach. The GSCs and U87MG cells were incubated in a 6-well plate and scratched with a sterile 100- μl pipette. Next, non-adherent cells and debris were discarded. Then, the GSCs and U87MG were treated with different concentrations of Nano-PTC209. Finally, the

wound closure of each group was photographed and analyzed under an inverted microscope (ZEISS Axiovert 200, Zeiss, Germany) at 4, 24, 48, and 72 h (Sahab-Negah et al. 2020).

Gelatin zymography

To detect the activity of the matrix metalloproteinases (MMP-9 and -2), gelatin zymography was used. GSCs and U87MG were treated with IC₅₀ and ½ IC₅₀ concentrations of Nano-PTC209 for 24 h. The cell culture supernatants containing 50 µg of total protein were electrophoresed in a 10% sodium dodecyl sulfate (SDS) polyacrylamide gel containing 10 mg/ml of gelatin followed by washing in 2% Triton X-100 three times to omit SDS. Next, to allow the digestion of the gelatin, the gel was incubated in a developing buffer composed of 50 mM Tris-HCl, 5 mM CaCl₂, and 0.2 M NaCl, 0.02% w/v NaN₃, pH 7.6, at 37 °C for 1 day. Then, the gel was stained with Coomassie Brilliant Blue R-250 (0.5% Coomassie Brilliant Blue R-250, 20% methanol, 10% acetic acid in dH₂O), and de-stained with washing buffer (25% ethanol plus 10% acetic acid in dH₂O). Finally, the stained gel was photographed and analyzed by ImageJ software.

Statistical analyses

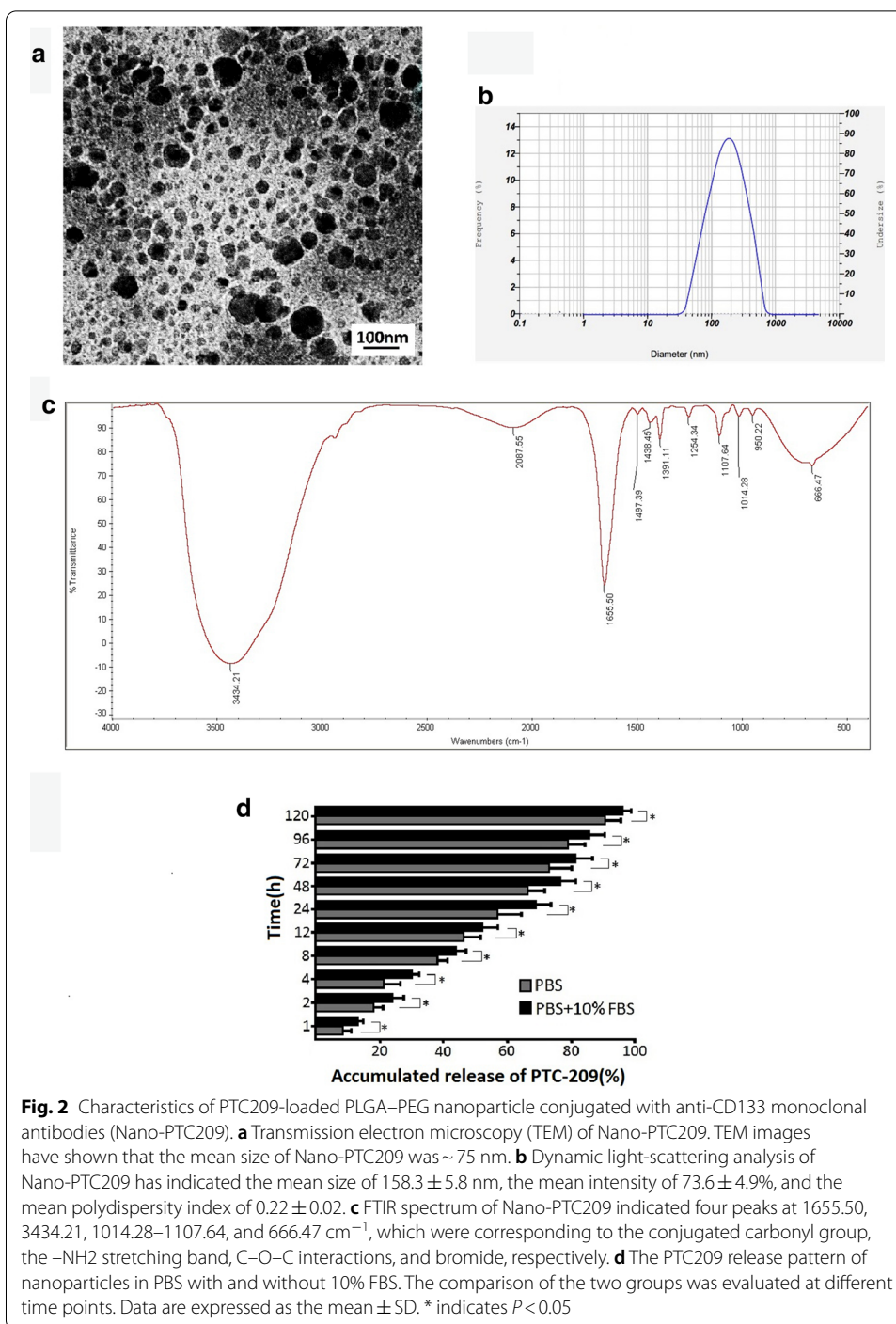
Statistical analyses were conducted by Prism version 6. All data are shown as mean ± standard deviation. Statistical differences were analyzed by the one-way analysis of variance (ANOVA) followed by the post hoc Tukey's test. Two-way repeated-measures ANOVA with Tukey post hoc tests was performed for migration assay data. The level of differences was regarded as significant at $P < 0.05$.

Results

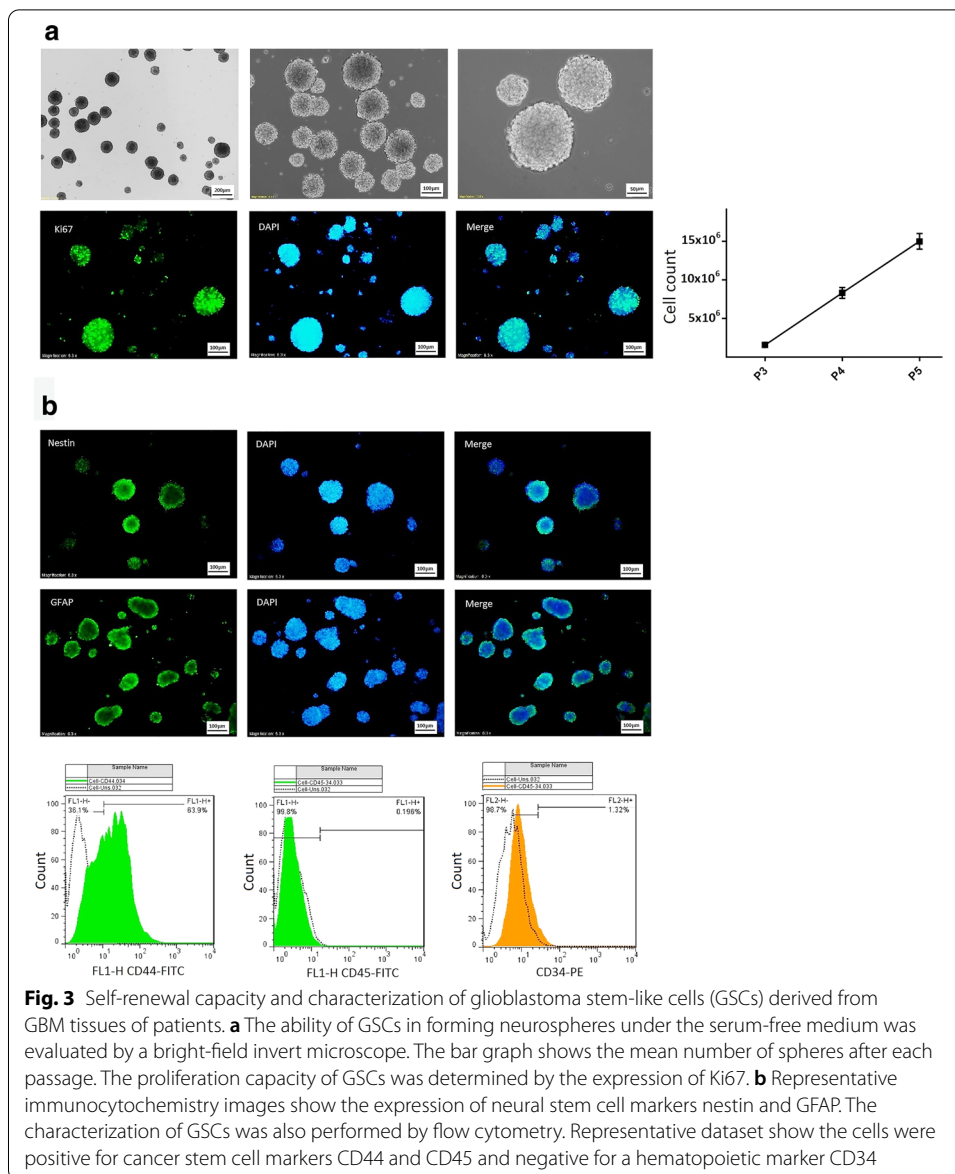
Characterization of Nano-PTC209

Both TEM and DLS were used to characterize Nano-PTC209. TEM images indicated that the diameter of nanoparticles was about ~75 nm (Fig. 2a). Furthermore, the analysis of DLS data indicated the mean size of 158.3 ± 5.8 nm (from 80 to ~1000 nm), the mean intensity of $73.6 \pm 4.9\%$, and the mean polydispersity index of 0.22 ± 0.02 (Fig. 2b). The zeta potential of Nano-PTC209 was ~ +0.1 mV. FTIR spectroscopy curves have shown the variation of functional-group frequencies of Nano-PTC209. FTIR spectrum showed a strong peak at 1655.50 cm^{-1} that exhibits the conjugated carbonyl group. The sharpness of this peak indicates the appropriate conjugation of Nano-PTC209. The peak at 3434.21 cm^{-1} depicts the -NH₂ stretching band, which is related to PLGA as well as conjugated antibody CD133 in this area. Furthermore, this peak shows amino acid density in the Nano-PTC209. The peaks range between 1014.28 and 1107.64 cm^{-1} belongs to C-O-C stretching, which is related to the ether structure of PEG in PLGA copolymer. The peak at 666.47 cm^{-1} is related to bromide, which exists in the structure of PTC209 (Fig. 2c).

The in vitro pattern of PTC209 release from Nano-PTC209 was evaluated in PBS with or without 10% FBS (Fig. 2d). The release of the drug was fast in the initial 12 h (~50%). After 24 h, the cumulative release reached ~65% in PBS with FBS, while similar to other intervals, the release pattern in PBS has shown a fewer amount with approximately 58% of drug release. The release of the nanoparticles (~80%)



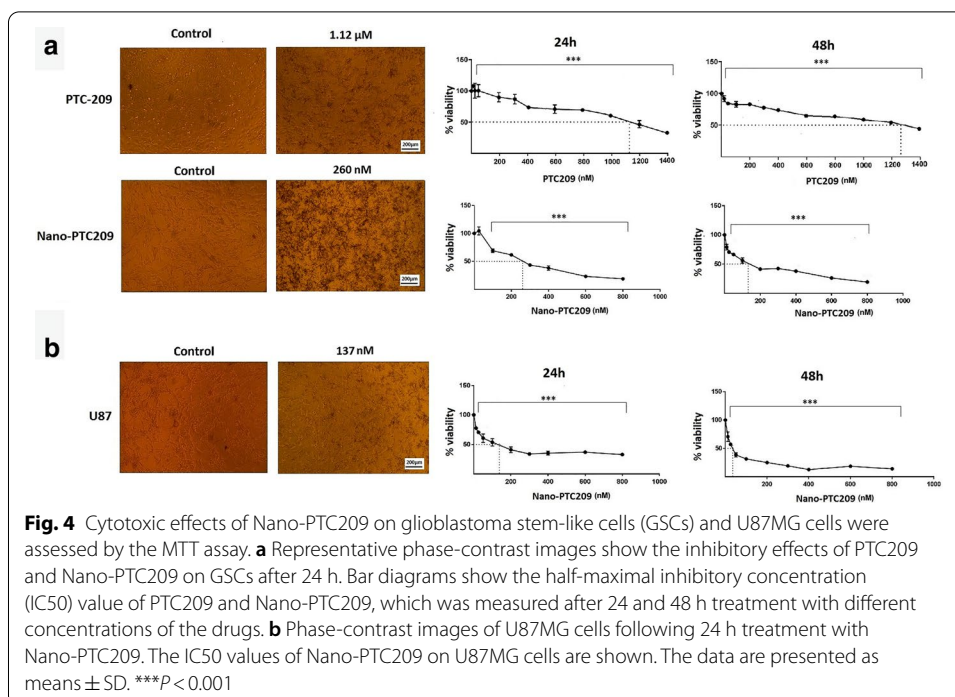
occurred in 96 h. PTC209 has exhibited similar sustained-release patterns that have been observed in both released media with a total release amount of 94% and 90% in PBS + 10 FBS and PBS, respectively, after 120 h (Fig. 2d).



Characterization and self-renewal of GSCs

The self-renewal capacity of GSCs was evaluated by neurosphere formation and the expression of ki67 antigen, respectively. The spherical colonies formed from GSCs within 5–7 days of cultivation, which could be passaged for 5 times (Fig. 3a). The proliferation capacity of GSCs is further examined by the expression of Ki67. Our results showed that the majority of GSCs expressed Ki67 (Fig. 3a).

Nestin and GFAP are common markers of GSCs and neural stem cells. Our results showed that GSCs were positive for nestin and GFAP (Fig. 3b). To characterize the GSCs, the specific markers, such as CD44, CD45, and CD34 were analyzed using flow cytometry. The GSCs expressed cancer stem cell markers CD44 and CD45 but did not express CD34, a hematopoietic marker (Fig. 3b).



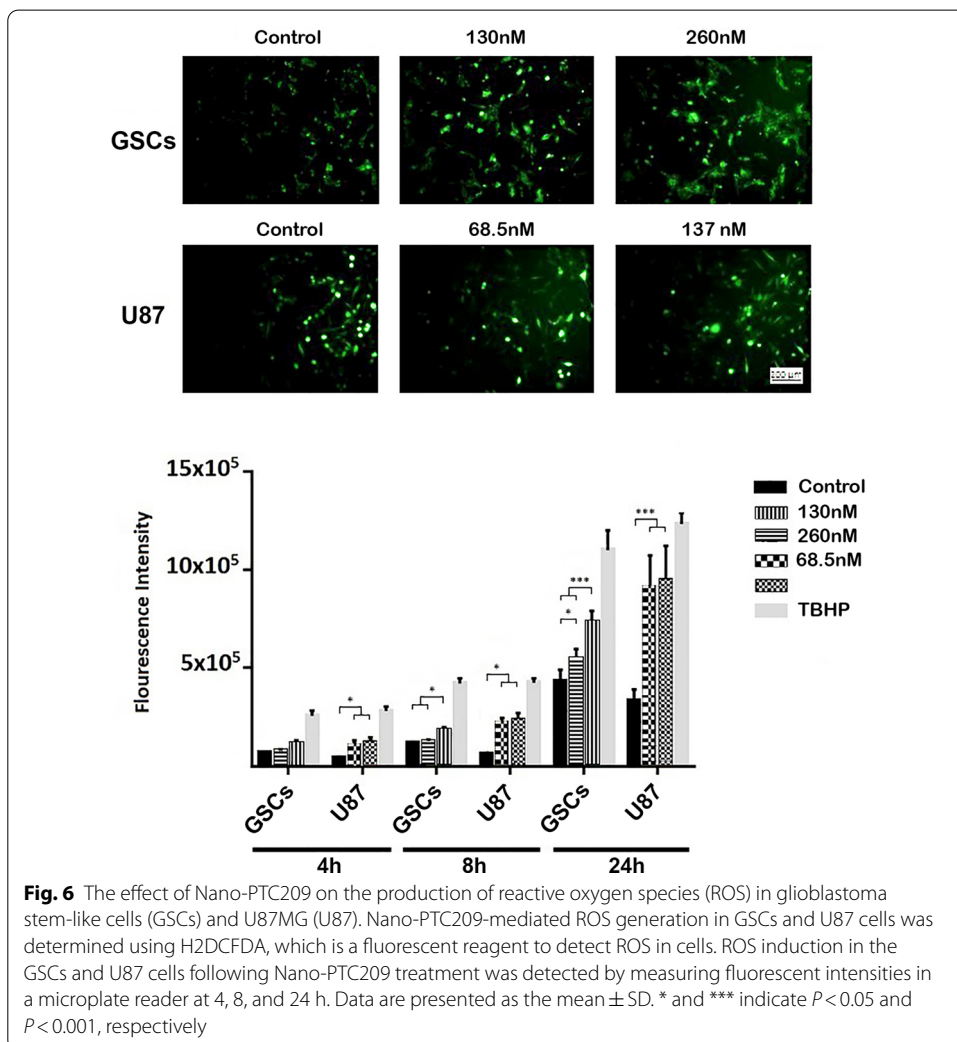
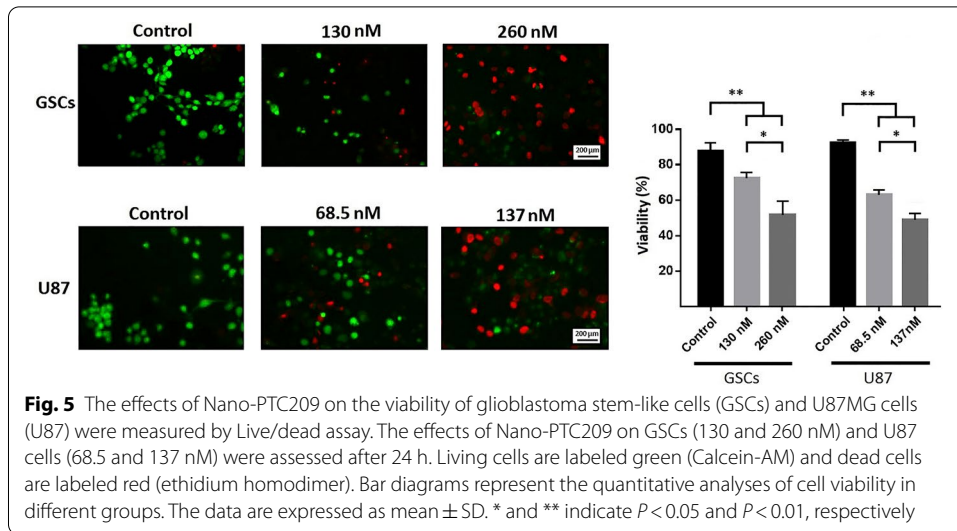
Tumor growth

Effect of Nano-PTC209 on cell proliferation

The functional effects of different doses of PTC209 and Nano-PTC209 on cell proliferation of the GSCs were tested using the MTT assay. The effects of PTC209 and Nano-PTC209 on the proliferation of GSCs were compared. The cell proliferation was evaluated after 24 and 48 h of GSC incubation with various doses of PTC209 or Nano-PTC209 (Fig. 4a). Both PTC209 and Nano-PTC209 significantly suppressed cell proliferation in a concentration- and time-dependent manner (*P* < 0.001). However, loading of PTC209 on the PLGA–PEG nanoparticle markedly increased the inhibitory effects of the substance on GSCs. The IC50 value of PTC209 was 1.25 μM after 24 h, which decreased to 1.12 μM after 48 h (Fig. 4a). The IC50 levels of Nano-PTC209 on GSCs were 260 and 150 nM following 24 and 48 h, respectively (Fig. 4a). We also investigated the effects of different concentrations of Nano-PTC209 on the proliferation of U87MG cells (Fig. 4b). Following 24 and 48 h of the incubation of cells with Nano-PTC209, the IC50 values were 137 and 43 nM, respectively (Fig. 4b).

Effect of Nano-PTC209 on cell viability

Using the live/dead assay, the effects of different concentrations of Nano-PTC209 on the cell viability of GSCs and U87MG were assessed (Fig. 5). The cell viability of GSCs treated with Nano-PTC209 at 130 and 260 nM for 24 h significantly reduced compared with the non-treated cells (Fig. 5; *P* < 0.01). Furthermore, the viability of U87MG cells treated with Nano-PTC209 at 68.5 and 137 nM significantly reduced compared with the control group (Fig. 5; *P* < 0.01). We also observed that the IC50 values of Nano-PTC209 (260 nM for GSCs and 137 nM for U87MG) significantly inhibited cell viability of GSCs and U87MG compared to ½ IC50 values.



Effect of Nano-PTC209 on ROS generation

The generation of ROS by GSCs and U87MG cells treated with Nano-PTC209 was measured. Nano-PTC209 induced a substantial increase in ROS levels in temporal- and dose-dependent manners in both GSCs and U87MG cells. The ROS level was significantly increased in the Nano-PTC209-treated GSCs at 130 and 260 nM after 8 ($P < 0.05$) and 24 h ($P < 0.001$) compared with the control groups (Fig. 6). The values of ROS were also greater in U87MG cells treated with Nano-PTC209 at values of 68.5 and 137 nM after 4 ($P < 0.05$), 8 ($P < 0.05$), and 24 h ($P < 0.001$) compared with the non-treated cells (Fig. 6).

Effect of Nano-PTC209 on molecular signaling of apoptosis

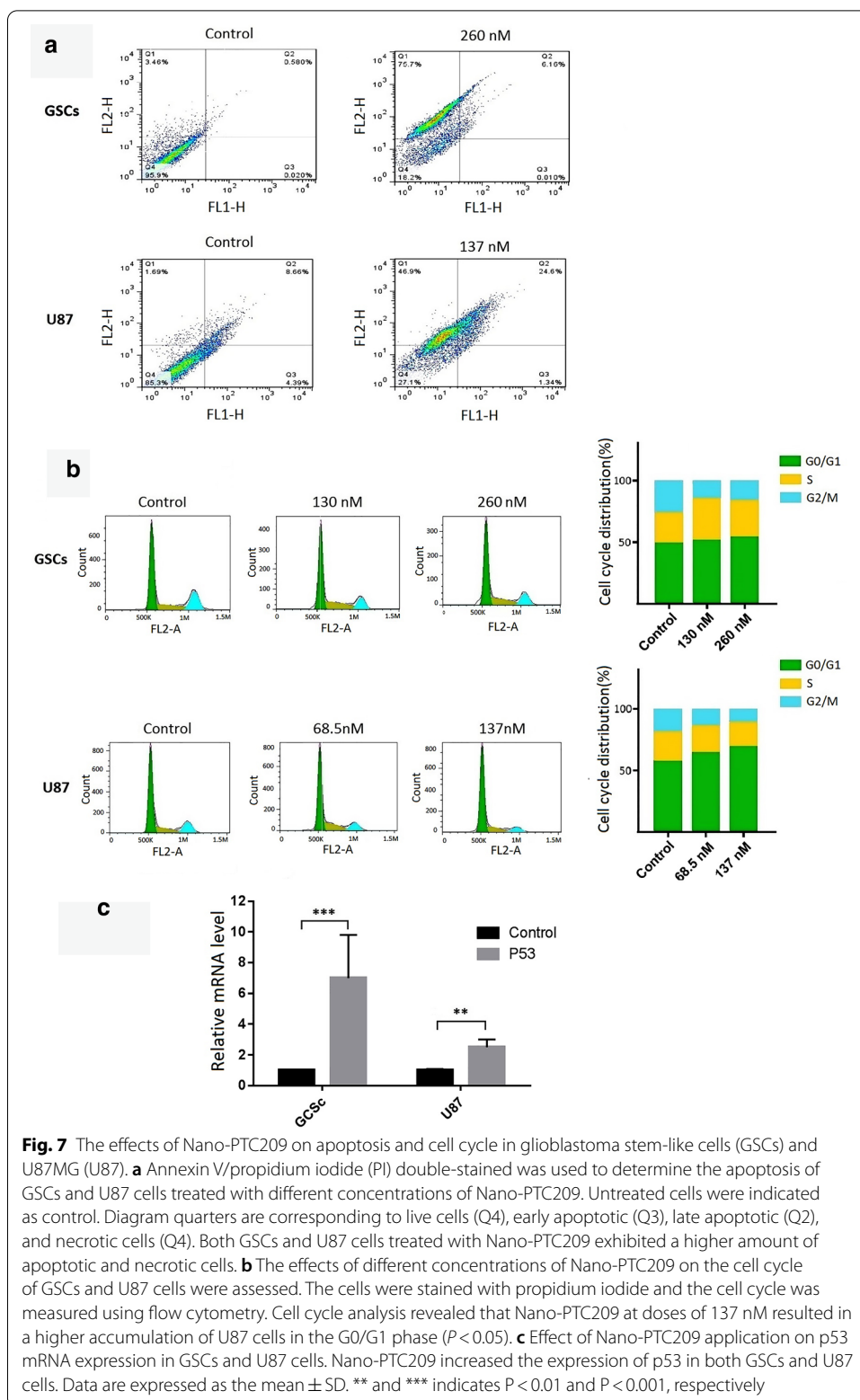
To quantify necrotic and apoptotic cells, GSCs and U87MG cells were incubated with different doses of Nano-PTC209 assessed by Annexin V-FITC-binding assay and PI staining. Treatment with Nano-PTC209 significantly enhanced the percentage of Annexin V-FITC-/PI-positive cells. The percentage of necrotic GSCs after treatment with Nano-PTC209 at 260 nM was ~76%. Furthermore, the number of late apoptotic and necrotic U87MG cells increased to ~25 and ~46%, respectively, when treated with Nano-PTC209 at 137 nM (Fig. 7a). We also examined cell cycle parameters in Nano-PTC209-treated GSCs and U87MG cells. Cell cycle analysis revealed that the administration of Nano-PTC209 at 137 nM resulted in a higher accumulation of U87MG cells in the G0/G1 phase (Fig. 7b; $P < 0.05$). Furthermore, the mRNA levels of P53 were evaluated in both GSCs and U87MG cells after the application of Nano-PTC209. Nano-PTC209 at concentrations of 260 and 137 nM significantly increased the levels of P53 in GSCs ($P < 0.001$) and U87MG cells (Fig. 7c; $P < 0.01$).

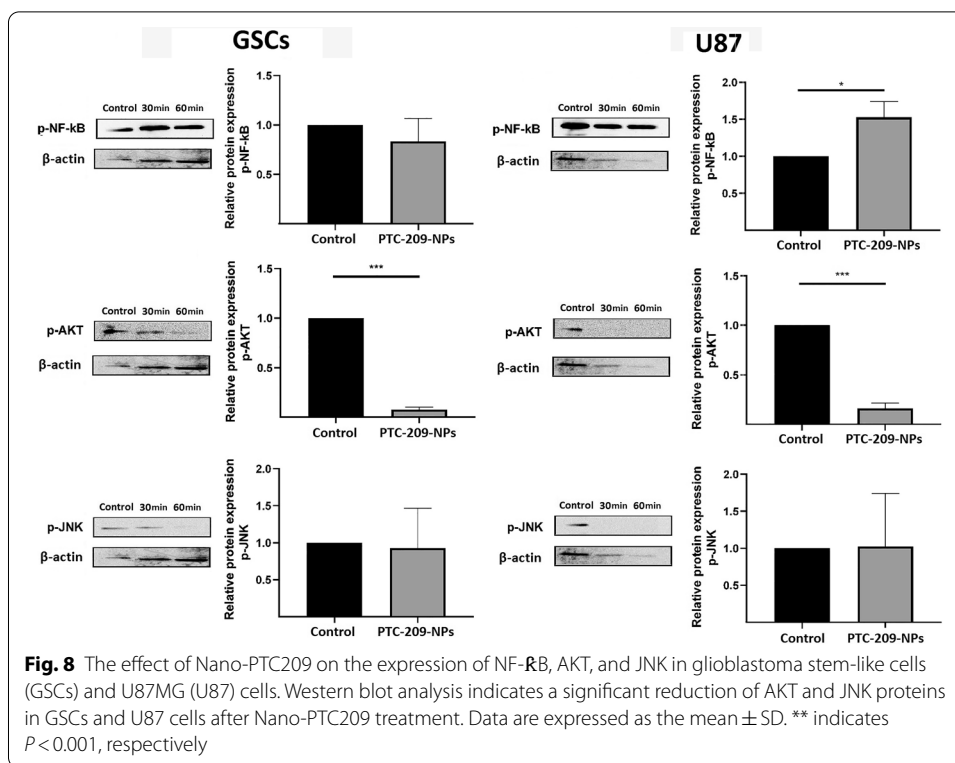
NF- κ B is an important transcription factor regulating tumor cell proliferation and apoptosis and phosphorylation of AKT and JNK signaling pathways modulate the GBM cell survival, growth, and migration (Engelman 2009). The application of Nano-PTC209 did not change the expression of NF- κ B in GSCs compared with untreated cells. The expression of NF- κ B significantly increased in Nano-PTC209 group compared to the control group (Fig. 8; $P < 0.05$). However, western blotting results showed that Nano-PTC209 significantly inhibited AKT and JNK phosphorylation in GSCs and U87MG cells (Fig. 8; $P < 0.001$).

Effect of Nano-PTC209 on migration and invasion

We assessed the effect of Nano-PTC209 on the migration ability of GSCs and U87MG cells using scratch wound assay. The migration of GSCs was inhibited by Nano-PTC209 (32.5 nM and 65 nM) in a concentration-dependent manner following 24, 48, and 72 h of treatment compared with the control group (Fig. 9a; $P < 0.01$). Besides, Nano-PTC209 (17.12 and 34.25 nM) exerted a dose-dependent inhibitory effect on U87MG cell migration after 24 ($P < 0.001$), 48, and 72 h ($P < 0.01$) of treatment compared with the control group (Fig. 9a).

To investigate whether Nano-PTC209 can suppress the secretion of MMP-2 and MMP-9, gelatin zymography of serum-free culture medium of untreated and Nano-PTC209-treated GSCs and U87MG cells were performed. The activation of both MMP-9 was significantly reduced in GSCs and U87MG cells treated with Nano-PTC209



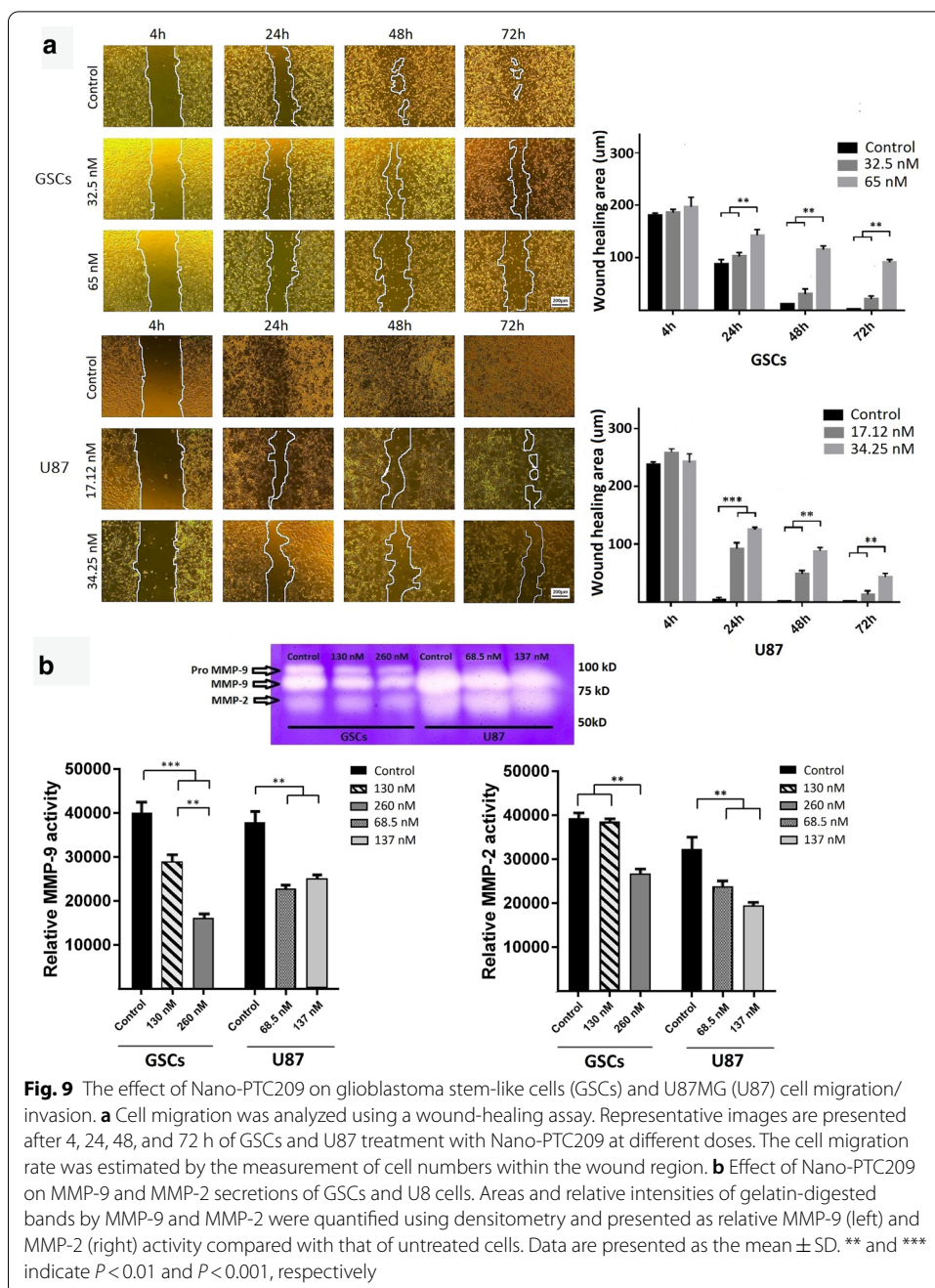


compared with the control groups (Fig. 9b; $P < 0.001$ and $P < 0.01$). The secretion of active MMP-9 in GSCs significantly inhibited by Nano-PTC209 at 260 nM compared to 130 nM ($P < 0.01$). Furthermore, Nano-PTC209 significantly decreased the secretion of MMP-2 in GSCs and U87MG cells compared with the control group ($P < 0.01$; Fig. 9b).

Discussion

The development of approaches targeting the GSCs may be a novel and promising therapeutic intervention in GBM (Eramo et al. 2006; Heddleston et al. 2009; Wang et al. 2017). The present study revealed potent antitumor effects of Nano-PTC209 against GSCs and U87MG cells. Nano-PTC209 decreased the viability and proliferation of GSCs isolated from human GBM and U87MG cells via the induction of apoptosis, the enhancement of p53 expression, the upregulation of ROS generation, and the regulation of the serine/threonine-protein kinases AKT1 as well as JNK pathway. Furthermore, Nano-PTC209 considerably inhibited the GSCs and U87MG migration/invasiveness, presumably via the inhibition of MMP-2 and MMP-9.

In keeping with our results, previous investigations revealed that the inhibition of BMI-1 by PTC209 reduces GBM cell behavior, such as proliferation, migration, and self-renewal through the restoration of transcriptional factors changed by hyperactive BMI-1 activity (Kong et al. 2018). However, high toxicity as well as the restricted blood-brain barrier permeability (due to high molecular weight and low liposolubility) could limit the therapeutic utility of PTC209 in the clinic (Pardridge et al. 2015; Srinivasan et al. 2017; Kong et al. 2018). Applying safe delivery systems in clinical use is considered a crucial issue. Several nanoparticles improve drug solubility, delivery, stability, and safety for the



drug delivery-based approach for the treatment of GBM (Jain, 2007; Kim et al. 2015). The challenge of delivering drugs to brain tumors and inadequate drug penetration from the blood–brain barrier has led to the development of nanoparticles in different fields. In this way, applying PLGA as an FDA-approved nanoparticle has been considerably enhanced to treat glioblastoma in recent years (Mahmoud et al. 2020; Roberts et al. 2020; Zhou et al. 2013). To minimize the toxicity of PTC209 as well as to improve targeted drug delivery, we designed PTC209-loaded PLGA–PEG nanoparticle conjugated with an anti-CD133 monoclonal antibody. To evaluate the antitumor activity of Nano-PTC209, primary glioblastoma

stem cells derived from patients as well as U87MG cells were treated with Nano-PTC209. The main rational reason to choose these cells was not only the evaluation of the heterogeneity between GBM cells but also the variability of cell response to the developed nanomedicine. PLGA–PEG copolymers, a suitable drug delivery system as tumor-targeting carriers, are promising biomaterials for the delivery and longer sustained and controlled release of both hydrophilic and hydrophobic substances (Veronese and Pasut 2005; Zhang et al. 2014; Xin et al. 2018). PEG has been mostly utilized as a component polymer in copolymer synthesis to enhance the efficiency of PLGA, decrease mechanical strength, and intensify degradable attribution (Guo et al. 2017). Using these copolymers decreases drug toxicity, enhances drug efficacy and improves drug delivery across the blood–brain barrier to the brain (Glaser et al. 2017; Velpurisiva et al. 2018; Hoyos-Ceballos et al. 2020). Furthermore, the conjugation of CD133 antibody with various nanoparticles has been suggested as an effective approach to enhance the efficacy and reduces the toxicity of different anti-GBM drugs, such as Temozolomide (Raucher et al. 2018). In the present study, the IC50 values of PTC209 for GSCs decreased from the micromolar range to the nanomolar levels when loaded into the PLGA–PEG nanoparticle, pointing to a greater drug efficacy with lower toxicity.

Our data revealed that targeting BMI-1 by Nano-PTC209 effectively inhibits GSCs and U87MG viability and self-renewal via the regulation of apoptosis through the modulation of p53 as well as the AKT1 and JNK pathways. The carcinogenesis of glioma is strongly correlated with the expression of BMI-1 gene expression and silencing of BMI-1 gene expression inhibits cell proliferation and induces the apoptosis of CD133-positive GBM cells (Hong et al. 2015). Despite considerable genomic heterogeneity among human GBM tumors, the main genetic events identified for GBM tumor formation include inactivation of the p53 tumor-suppressor pathways, activation of the PI3 kinase/AKT pathway, and augmentation and activation of receptor tyrosine kinase genes (Network, 2008). The tumor-suppressor protein p53 regulates a variety of cellular responses in GBM, including apoptosis, angiogenesis, and genomic stability, as well as the maintenance of the tumor microenvironment (Zhang et al. 2014). Dysregulation of the p53 pathway is reported in approximately 90% of patients with GBM, which is accompanied by poor prognosis (Touat et al. 2017). BMI-1 deficiency resulted in the activation of the p53 pathway (Chatoo et al. 2009). Higher BMI-1 expression in tumors activated the cell proliferation through the inhibition of tumor-suppressor protein MEK1-stimulated apoptosis as well as the activation of different apoptosis-associated mediators, including p53 genes (Kim et al. 2018). Furthermore, JNK plays an important role in apoptosis and cell death as well as migration/invasion of GBM cells and has crosstalk with the Akt signaling pathway (Zhao et al. 2016). BMI-1-induced phosphorylation of Akt and JNK plays a crucial role in BMI-1-mediated tumorigenesis and migration in GBM cells and GSCs (Abdoun et al. 2009; Matsuda et al. 2012). Mutual interaction between the JNK signaling pathway and the Akt pathway promotes tumorigenesis in GBM (Van Anh et al. 2014). The activation of JNK and AKT signaling pathways is implicated in GSCs survival and correlated with poor outcomes in patients with GBM (Matsuda et al. 2012).

Furthermore, the expression of BMI-1 regulates ROS generation (Liu et al. 2009). The cellular redox impairment facilitates GBM cell growth and invasion and the excessive ROS production contributes to the induction of apoptosis and cell cycle arrest as well as the

prevention of invasion/migration of GBM (Salazar-Ramiro et al. 2016; Rinaldi et al. 2016). Besides, both MMP-2 and MMP-9 control the GBM cell proliferation and invasiveness through the modulation of tumor angiogenesis (Du et al. 2008; Veeravalli et al. 2012). In addition to cell proliferation, targeting BMI-1 by Nano-PTC209 may effectively inhibit the migration/invasiveness of GSCs and GBM cells via the modulation of ROS and MMP.

Conclusion

Taken together, the present investigation is the first to study the effect of a BMI-1 inhibitor loaded into the PLGA–PEG nanoparticles conjugated with an anti-CD133 monoclonal antibody on GSCs and GBM cells. Nano-PTC209 was suitably developed for the delivery of PTC209 to GSCs and GBM cells. The IC₅₀ value of Nano-PTC209 on GSCs was remarkably lower than PTC209. Our data revealed that Nano-PTC209 effectively inhibits the viability, proliferation, and migration/invasiveness of GSCs and U87MG cells via several molecular mechanisms, including the induction of apoptosis and cell cycle arrest, the enhancement of p53 mRNA expression and ROS generation, and the inhibition of JNK and AKT phosphorylation. Furthermore, Nano-PTC209 targets the invasiveness of GSCs and U87MG via inhibition of MMP-9 and MMP-2 secretions. Further, *in vivo* studies are required to investigate the anti-proliferative effect of Nano-PTC209 on GBM and to validate its anticancer potential in clinical settings. Furthermore, investigations to evaluate Nano-PTC209 uptake mechanisms/pathways for understanding and explanation of efficacy/efficiency of the drug are needed.

Abbreviations

ANOVA: One-way analysis of variance; BMI-1: Human B cell-specific Moloney murine leukemia virus integration site 1; DMSO: Dimethyl sulfoxide; DLS: Dynamic light scattering; FITC: Fluorescein isothiocyanate; FTIR: Fourier Transform Infrared Spectroscopy; GBM: Glioblastoma multiforme; GSCs: Glioblastoma stem-like cells; IC₅₀: Half-maximal inhibitory concentration; JNK: c-Jun N-terminal kinases; MMP: Matrix metalloproteinases; Nano-PTC209: PTC209 loaded into a PLGA–PEG nanoparticle conjugated with CD133 antibody; PEG–PLGA: Polyethylene glycol–polylactic acid-co-glycolic acid; PVDF: Polyvinylidene fluoride; RT-PCR: Real-time polymerase chain reaction; ROS: Reactive oxygen species; SDS: Sodium dodecyl sulfate; TEM: Transmission electron microscopy.

Acknowledgements

NA.

Authors' contributions

EP, FA, and MJ contributed equally to this study. EP, FA, MSA, GT, and SG performed the experiments, collected and analyzed data. EP, SSN, and AG contributed to experimental design and its implementation. FS provided tumor tissues. SSN and AG contributed to the interpretation of the data and wrote a preliminary draft of the manuscript. All the authors read and approved the final manuscript.

Funding

Open Access funding enabled and organized by Projekt DEAL. This study was supported by the National Institute for Medical Research (NIMAD; 964650) to AG.

Ethics approval and consent to participate

Ethical approval was obtained from the Ethics Committee of Shefa Neuroscience Research Center, Tehran, Iran.

Consent for publication

The consent to publish this manuscript has been obtained from all the authors.

Competing interests

None.

Author details

¹ Department of Radiopharmacy, Faculty of Pharmacy, Tehran University of Medical Sciences, Tehran, Iran. ² Neuroscience Research Center, Mashhad University of Medical Sciences, Mashhad, Iran. ³ Department of Neuroscience, Faculty of Medicine, Mashhad University of Medical Sciences, Mashhad, Iran. ⁴ Student Research Committee, Mashhad University of Medical Sciences, Mashhad, Iran. ⁵ Department of Medical Biochemistry, Faculty of Medicine, Mashhad University of Medical Sciences, Mashhad, Iran. ⁶ Department of Pathobiology, Faculty of Veterinary Medicine, Shiraz University,

Shiraz, Iran. ⁷ Department of Neurosurgery, Faculty of Medicine, Mashhad University of Medical Sciences, Mashhad, Iran. ⁸ Shefa Neuroscience Research Center, Khatam Alanbia Hospital, Tehran, Iran. ⁹ Department of Neurosurgery and Department of Neurology, Westfälische Wilhelms-Universität, Münster, Germany. ¹⁰ Epilepsy Research Center, Westfälische Wilhelms-Universität Münster, 48149 Münster, Germany.

Received: 16 November 2020 Accepted: 27 January 2021

Published online: 06 February 2021

References

- Abdouh M, Facchino S, Chatoov W, Balasingam V, Ferreira J, Bernier G. BMI1 sustains human glioblastoma multiforme stem cell renewal. *J Neurosci*. 2009;29:8884–96.
- Abouelmagd SA, Sun B, Chang AC, Ku YJ, Yeo Y. Release kinetics study of poorly water-soluble drugs from nanoparticles: are we doing it right? *Mol Pharm*. 2015;12(3):997–1003.
- Agarwal S, Mohamed MS, Mizuki T, Maekawa T, Sakthi KD. Chlorotoxin modified morusin-PLGA nanoparticles for targeted glioblastoma therapy. *J Mater Chem B*. 2019;7(39):5896–919.
- Baxter PA, Lin Q, Mao H, Kogiso M, Zhao X, Liu Z, et al. Silencing BMI1 eliminates tumor formation of pediatric glioma CD133+ cells not by affecting known targets but by down-regulating a novel set of core genes. *Acta Neuropathol Commun*. 2014;2:160.
- Chatoov W, Abdouh M, David J, Champagne M-P, Ferreira J, Rodier F, et al. The polycomb group gene Bmi1 regulates antioxidant defenses in neurons by repressing p53 pro-oxidant activity. *J Neurosci*. 2009;29:529–42.
- Di Croce L, Helin K. Transcriptional regulation by Polycomb group proteins. *Nat Struct Mol Biol*. 2013;20:1147.
- Du R, Petritsch C, Lu K, Liu P, Haller A, Ganss R, et al. Matrix metalloproteinase-2 regulates vascular patterning and growth affecting tumor cell survival and invasion in GBM. *Neuro-oncology*. 2008;10:254–64.
- Engelman JA. Targeting PI3K signalling in cancer: opportunities, challenges and limitations. *Nat Rev Cancer*. 2009;9:550–62.
- Eramo A, Ricci-Vitiani L, Zeuner A, Pallini R, Lotti F, Sette G, et al. Chemotherapy resistance of glioblastoma stem cells. *Cell Death Differ*. 2006;13:1238–41.
- Glaser T, Han I, Wu L, Zeng X. Targeted nanotechnology in glioblastoma multiforme. *Front Pharmacol*. 2017;8:166.
- Granz CL, Gorji A. Dental stem cells: The role of biomaterials and scaffolds in developing novel therapeutic strategies. *World Journal of Stem Cells*. 2020;12(9):897–921.
- Guo X, Zhu X, Gao J, Liu D, Dong C, Jin X. PLGA nanoparticles with CD133 aptamers for targeted delivery and sustained release of propranolol to hemangioma. *Nanomedicine*. 2017;12:2611–24.
- Hanif F, Muzaffar K, Perveen K, Malhi SM, Simjee SU. Glioblastoma multiforme: a review of its epidemiology and pathogenesis through clinical presentation and treatment. *Asian Pacific J Cancer Prev APJCP*. 2017;18:3.
- Heddleston JM, Li Z, McLendon RE, Hjelmeland AB, Rich JN. The hypoxic microenvironment maintains glioblastoma stem cells and promotes reprogramming towards a cancer stem cell phenotype. *Cell Cycle*. 2009;8:3274–84.
- Hong Y, Shang C, Xue Y-X, Liu Y-H. Silencing of Bmi-1 gene enhances chemotherapy sensitivity in human glioblastoma cells. *Med Sci Monit*. 2015;21:1002.
- Hoyos-Ceballos GP, Ruozzi B, Ottonelli I, Da Ros F, Vandelli MA, Forni F, et al. PLGA-PEG-ANG-2 nanoparticles for blood-brain barrier crossing: proof-of-concept study. *Pharmaceutics*. 2020;12:72.
- Jain K. Use of nanoparticles for drug delivery in glioblastoma multiforme. *Expert Rev Neurother*. 2007;7:363–72.
- Kim S-S, Harford JB, Pirollo KF, Chang EH. Effective treatment of glioblastoma requires crossing the blood–brain barrier and targeting tumors including cancer stem cells: the promise of nanomedicine. *Biochem Biophys Res Commun*. 2015;468:485–9.
- Kim W, Youn H, Lee S, Kim E, Kim D, Lee JS, et al. RNF138-mediated ubiquitination of rp53 is required for resistance of glioblastoma cells to radiation-induced apoptosis. *Exp Mol Med*. 2018;50:434.
- Kong Y, Ai C, Dong F, Xia X, Zhao X, Yang C, et al. Targeting of BMI-1 with PTC-209 inhibits glioblastoma development. *Cell Cycle*. 2018;17:1199–211.
- Kreso A, Van Galen P, Pedley NM, Lima-Fernandes E, Frelin C, Davis T, et al. Self-renewal as a therapeutic target in human colorectal cancer. *Nat Med*. 2014;20:29.
- Liao W, Fan S, Zheng Y, Liao S, Xiong Y, Li Y, Liu J. Recent advances on glioblastoma multiforme and nano-drug carriers: a review. *Curr Med Chem*. 2019;26(31):5862–74.
- Lim SH, Jang J, Park JO, Kim K-M, Kim ST, Park YS, et al. CD133-positive tumor cell content is a predictor of early recurrence in colorectal cancer. *J Gastrointest Oncol*. 2014;5:447.
- Liu J, Cao L, Chen J, Song S, Lee IH, Quijano C, et al. Bmi1 regulates mitochondrial function and the DNA damage response pathway. *Nature*. 2009;459:387–92.
- Mahmoud BS, AlAmri AH, McConville C. Polymeric nanoparticles for the treatment of malignant gliomas. *Cancers*. 2020;12:175.
- Matsuda K-I, Sato A, Okada M, Shibuya K, Seino S, Suzuki K, et al. Targeting JNK for therapeutic depletion of stem-like glioblastoma cells. *Sci Rep*. 2012;2:516.
- Network CGAR. Comprehensive genomic characterization defines human glioblastoma genes and core pathways. *Nature*. 2008;455:1061.
- Pardridge WM. Blood–brain barrier endogenous transporters as therapeutic targets: a new model for small molecule CNS drug discovery. *Expert Opin Therap Targets*. 2015;19:1059–72.
- Qazi M, Vora P, Venugopal C, Sidhu S, Moffat J, Swanton C, et al. Intratumoral heterogeneity: pathways to treatment resistance and relapse in human glioblastoma. *Ann Oncol*. 2017;28:1448–56.
- Raucher D, Dragojevic S, Ryu J. Macromolecular drug carriers for targeted glioblastoma therapy: preclinical studies, challenges, and future perspectives. *Front Oncol*. 2018;8:624.
- Roberts R, Smyth JW, Will J, Roberts P, Grek CL, Ghatnekar GS, et al. Development of PLGA nanoparticles for sustained release of a connexin43 mimetic peptide to target glioblastoma cells. *Mater Sci Eng C*. 2020;108:110191.

- Rinaldi M, Caffo M, Minutoli L, Marini H, Abbritti RV, Squadrito F, et al. ROS and brain gliomas: an overview of potential and innovative therapeutic strategies. *Int J Mol Sci*. 2016;17:984.
- Sahab-Negah S, Ariakia F, Jalili-Nik M, Afshari AR, Salehi S, Samini F, Rajabzadeh G, Gorji A. Curcumin loaded in niosomal nanoparticles improved the anti-tumor effects of free curcumin on glioblastoma stem-like cells: an in vitro study. *Mol Neurobiol*. 2020;57(8):3391–411.
- Sahab Negah S, Shirzad MM, Biglari G, Naseri F, Hosseini Ravandi H, Hassani Dooghabadi A, Gorji A. Transplantation of R-GSik scaffold with mesenchymal stem cells improves neuroinflammation in a traumatic brain injury model. *Cell Tissue Res*. 2020. <https://doi.org/10.1007/s00441-020-03247-0>.
- Salazar-Ramiro A, Ramírez-Ortega D, Pérez de la Cruz V, Hernández-Pedro NY, González-Esquivel DF, Sotelo J, et al. Role of redox status in development of glioblastoma. *Front Immunol*. 2016;7:156.
- Sebaugh JL. Guidelines for accurate EC50/IC50 estimation. *Pharm Stat*. 2011;10(2):128–34.
- Senapati S, Mahanta AK, Kumar S, Maiti P. Controlled drug delivery vehicles for cancer treatment and their performance. *Signal Trans Targeted Ther*. 2018;3:1–19.
- Shevchenko V, Arnotskaya N, Pak O, Sharma A, Sharma HS, Khotimchenko Y, et al. Molecular determinants of the interaction between glioblastoma CD133+ cancer stem cells and the extracellular matrix. *Int Rev Neurobiol*. 2020;151:155–69.
- Srinivasan M, Bharali DJ, Sudha T, Khedr M, Guest I, Sell S, et al. Downregulation of Bmi1 in breast cancer stem cells suppresses tumor growth and proliferation. *Oncotarget*. 2017;8:38731.
- Sulaiman S, Arafat K, Itratni R, Attoub S. PTC-209 anti-cancer effects involved the inhibition of STAT3 phosphorylation. *Front Pharmacol*. 2019;10:1199.
- Touat M, Idbaih A, Sanson M, Ligon K. Glioblastoma targeted therapy: updated approaches from recent biological insights. *Ann Oncol*. 2017;28:1457–72.
- van Anh V, Lee J-W, Lee HJ, Chun W, Lim SY, Kim S-S. Inhibition of JNK potentiates temozolomide-induced cytotoxicity in U87MG glioblastoma cells via suppression of Akt phosphorylation. *Anticancer Res*. 2014;34:5509–15.
- Veeravalli KK, Rao JS. MMP-9 and uPAR regulated glioma cell migration. *Cell Adhesion Migration*. 2012;6:509–12.
- Velpurisiva P, Piel BP, Lepine J, Rai P. GSK461364A, a polo-like kinase-1 inhibitor encapsulated in polymeric nanoparticles for the treatment of glioblastoma multiforme (GBM). *Bioengineering*. 2018;5:83.
- Venugopal C, Li N, Wang X, et al. Bmi1 marks intermediate precursors during differentiation of human brain tumor initiating cells. *Stem Cell Res*. 2012;8(2):141–53. <https://doi.org/10.1016/j.scr.2011.09.008>.
- Veronese FM, Pasut G. PEGylation, successful approach to drug delivery. *Drug Discovery Today*. 2005;10:1451–8.
- Vora P, Seyfrid M, Venugopal C, et al. Bmi1 regulates human glioblastoma stem cells through activation of differential gene networks in CD133+ brain tumor initiating cells. *J Neurooncol*. 2019;143(3):417–28.
- Wait SD, Prabhu RS, Burri SH, Atkins TG, Asher AL. Polymeric drug delivery for the treatment of glioblastoma. *Neuro Oncol*. 2015;17:9–23.
- Wang MC, Li CL, Cui J, Jiao M, Wu T, Jing L, et al. BMI-1, a promising therapeutic target for human cancer. *Oncol Lett*. 2015;10:583–8.
- Wang Q, Li Z, Wu Y, Huang R, Zhu Y, Zhang W, et al. Pharmacological inhibition of Bmi1 by PTC-209 impaired tumor growth in head neck squamous cell carcinoma. *Cancer Cell Int*. 2017;17:107.
- Xin L, Zhang H-T, Yang W-F, Li Y-F, Liu C. Evaluation of METase-pemetrexed-loaded PEG–PLGA nanoparticles modified with anti-CD133–scFV for treatment of gastric carcinoma. *Bioscience Rep*. 2018. <https://doi.org/10.1042/BSR20171001>.
- Yoshimoto K, Ma X, Guan Y, Mizoguchi M, Nakamizo A, Amano T, et al. Expression of stem cell marker and receptor kinase genes in glioblastoma tissue quantified by real-time RT-PCR. *Brain Tumor Pathol*. 2011;28:291–6.
- Zhang K, Tang X, Zhang J, Lu W, Lin X, Zhang Y, et al. PEG–PLGA copolymers: their structure and structure-influenced drug delivery applications. *J Control Release*. 2014;183:77–86.
- Zhao H-F, Wang J, Jiang H-R, Chen Z-P, To SST. PI3K p110 β isoform synergizes with JNK in the regulation of glioblastoma cell proliferation and migration through Akt and FAK inhibition. *J Exp Clin Cancer Res*. 2016;35:78.
- Zhou J, Patel TR, Sirianni RW, Strohbehm G, Zheng MQ, Duong N, Schafbauer T, Huttner AJ, Huang Y, Carson RE, Zhang Y. Highly penetrative, drug-loaded nanocarriers improve treatment of glioblastoma. *Proc Natl Acad Sci*. 2013;110(11):11751–6.

Publisher's Note

Springer Nature remains neutral with regard to jurisdictional claims in published maps and institutional affiliations.

Ready to submit your research? Choose BMC and benefit from:

- fast, convenient online submission
- thorough peer review by experienced researchers in your field
- rapid publication on acceptance
- support for research data, including large and complex data types
- gold Open Access which fosters wider collaboration and increased citations
- maximum visibility for your research: over 100M website views per year

At BMC, research is always in progress.

Learn more biomedcentral.com/submissions

